Production of long-lived atomic vapor inside high-density buffer gas

A. O. Sushkov[1,*] and D. Budker[1,2]
[1]*Department of Physics, University of California at Berkeley, Berkeley, California 94720-7300, USA*
[2]*Nuclear Science Division, Lawrence Berkeley National Laboratory, Berkeley, California 94720, USA*
(Received 25 January 2008; published 9 April 2008)

Atomic vapor of four different paramagnetic species: gold, silver, lithium, and rubidium, is produced and studied inside several buffer gases: helium, nitrogen, neon, and argon. The paramagnetic atoms are injected into the buffer gas using laser ablation. Wires with diameters 25, 50, and 100 μm are used as ablation targets for gold and silver; bulk targets are used for lithium and rubidium. The buffer gas cools and confines the ablated atoms, slowing down their transport to the cell walls. Buffer gas temperatures between 20 and 295 K and densities between 10^{16} cm^{-3} and 2×10^{19} cm^{-3} are explored. Peak paramagnetic atom densities of 10^{11} cm^{-3} are routinely achieved. The longest observed paramagnetic vapor density decay times are 110 ms for silver at 20 K and 4 ms for lithium at 120 K. The candidates for the principal paramagnetic-atom loss mechanism are impurities in the buffer gas, dimer formation, and atom loss on sputtered clusters.

DOI: 10.1103/PhysRevA.77.042707 PACS number(s): 34.50.−s, 32.10.−f, 33.57.+c, 37.20.+j

I. INTRODUCTION

The ability to achieve long-lived coherences in an ensemble of atoms or molecules is at the core of many of today's atomic physics experiments. Such experiments are at the forefront of both technological applications, such as atomic magnetometers [1,2], spin-exchange optical pumping of noble-gas nuclei [3], and quantum computation [4], and more fundamental research, such as tests of Lorentz invariance [5,6] and searches for violation of the discrete symmetries of nature [7]. In room-temperature experiments involving ground-state electron-spin coherences, alkali-metal atoms are most often used inside sealed vapor cells, which are either coated with an antirelaxation material, such as paraffin [8,9], or filled with a buffer gas, such as helium [3]. An alkali-metal atom inside such a cell is prepared in a coherent state by optical pumping; the coherences here are between ground-state magnetic sublevels. In an antirelaxation coated cell, it can then experience thousands of velocity-changing collisions with the cell walls before decohering. Coherence times of 500 ms have been demonstrated in such cells; see, for example, Ref. [10]. In a buffer-gas-filled cell, depolarization due to cell-wall collisions is suppressed, since the alkali-metal atoms no longer travel ballistically, but have to diffuse inside the buffer gas, whose density ranges typically from 10^{16} cm^{-3} up to 10^{19} cm^{-3}. However, as the buffer-gas density is increased, slowing down alkali-metal diffusion, collisional decoherence starts to dominate. This refers to spin relaxation of the alkali-metal atom in a collision with a buffer-gas atom due to spin-orbit interaction [11]. Coherence times of 20 ms have been achieved in buffer-gas filled cells [12,13]. Collisional relaxation cross sections of the alkali-metal atoms have been studied at room temperature and above, but not for lower temperatures. The reason for this is the insufficient saturated vapor pressure of the alkali metals below room temperature, which makes experiments with sealed vapor cells extremely hard.

There are, however, compelling theoretical reasons to believe that buffer-gas collisional relaxation cross sections should drop quickly as the temperature is lowered. This relaxation occurs due to the spin-rotation coupling (which arises from spin-orbit interaction [14–16]):

$$H = \gamma(R)\boldsymbol{S}\cdot\boldsymbol{N}, \tag{1}$$

where γ is the interaction strength, R is the distance between the colliding alkali-metal and buffer-gas atoms, $\boldsymbol{S}$ is the alkali-metal electron spin, and $\boldsymbol{N}$ is the rotational angular momentum of their relative motion. In the present work, helium is used as the buffer gas at cryogenic temperatures, and several other buffer gases are used at higher temperatures also. Formation of van der Waals molecules is neglected [17], and the spin-relaxation cross section can be evaluated in the semiclassical binary collision approximation

$$\sigma(E) = \frac{8\pi M^2}{3\hbar^4}\int_0^\infty b^3 db\left|\int_{r_0}^\infty \frac{\gamma(R)dR}{\sqrt{(1-b^2/R^2)-V(R)/E}}\right|^2, \tag{2}$$

where $V(R)$ is the interatomic potential, b is the impact parameter, E is the collision energy, r_0 is the distance of closest approach, and M is the reduced mass of the colliding atoms. The key input into this expression is the R dependence of $\gamma(R)$. It is possible to estimate $\gamma(R)$ by approximating the alkali-metal valence electron wave function at large distances r from the core by the hydrogenic expression (in atomic units)

$$\phi(r) \propto r^{\nu-1}e^{-r/\nu}, \tag{3}$$

where ν is the effective principal quantum number of the ground-state valence electron. Using the results of Ref. [15], $\gamma(R)$ can be estimated with logarithmic precision, resulting in the exponential R dependence

$$\gamma(R) \propto e^{-2R/\nu}. \tag{4}$$

This is in good agreement with the results of numerical calculations presented in Ref. [15]. It is already possible to argue why the spin-relaxation cross section decreases rapidly at low temperatures. As the temperature is lowered, the collision energy decreases, and the alkali-metal-helium closest approach distance increases due to repulsion between the He and the valence electron. Since the spin-rotation interaction

*alexsushkov@berkeley.edu

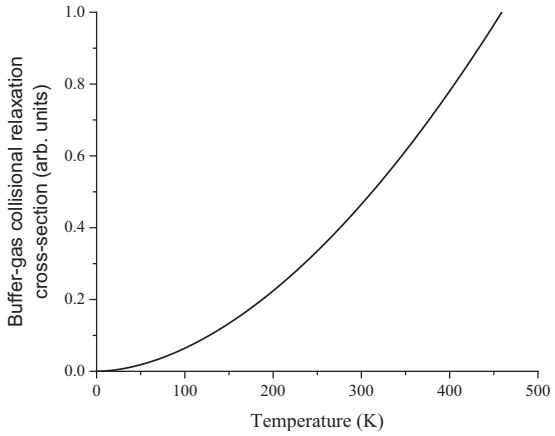

FIG. 1. The estimated scaling of Rb-He spin-relaxation cross section with temperature.

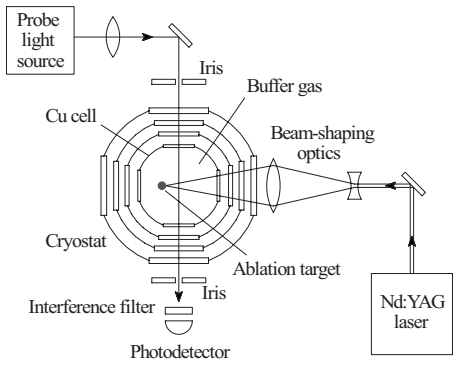

FIG. 2. A schematic top view of the experimental setup.

of Eq. (4) drops exponentially, the corresponding spin-flip cross section also decreases. We make no attempt at calculating the magnitude of the relaxation cross section; instead we estimate its temperature dependence, using Eq. (4) and the interatomic potential of the form

$$V(R) = AR^{2\nu-2}e^{-2R/\nu} - \frac{C_6}{R^6}, \tag{5}$$

where the first (repulsion) term is taken to be proportional to the probability density of the alkali-metal electron at the location of the helium atom, and the second term is the van der Waals attraction. The van der Waals coefficient C_6 is known from experiment, and the parameter A fitted to reproduce the experimentally observed potential minimum. The result of numerical integration of Eq. (2) is plotted in Fig. 1 for Rb-He collisions. The interatomic potential parameters are obtained from Refs. [18,19].

If indeed, as shown in Fig. 1, the buffer-gas collisional relaxation cross section drops rapidly with decreasing temperature, extremely long ground-state electron spin-relaxation times can be achieved in alkali-metal atoms inside high-density helium buffer gas at low temperature. There are, of course, other spin-relaxation mechanisms that will limit the achievable relaxation times, such as spin destruction and spin exchange in collisions between the alkali-metal atoms themselves. It is much harder to estimate the behavior of the corresponding cross sections at low temperatures, and the region between 4 and 300 K remains experimentally unexplored. Data are available at higher temperatures for a variety of other buffer gases (such as N_2, ^{3}He, Xe); a discussion of the relevant temperature dependences is given in Ref. [20]. We note, however, that our simple model is not applicable in these cases, where other effects, such as formation of van der Waals molecules, contribute to the spin-destruction cross section.

As mentioned above, the reason for scarcity of experimental data below room temperature is the vanishing saturated vapor pressure of the alkali metals. There has, however, been some recent experimental effort in this direction. One technique that has been used to study alkali-metal atoms in helium-filled cells at cryogenic conditions is loading by light-induced atomic desorption (LIAD) from the liquid-helium film that covers the cell walls below the helium superfluid-transition temperature [21,22]. These experiments were performed at 1.85 K, and spin-relaxation times of minutes and even longer can be inferred from the data. This already supports the theoretical estimates outlined above. Another technique that has recently been well developed is production of cold atomic and molecular beams by laser ablation inside helium buffer gas at temperatures on the order of 5 K [23]. The same technique has also been used for loading atoms and molecules into magnetic traps [24,25]. The experiments described in the present paper fall somewhere in the middle between these techniques. We use laser ablation to produce high densities of atomic species inside helium buffer gas in a range of temperatures between 20 and 300 K, but, in addition to cooling the ablated atoms, the buffer gas also confines them by slowing down transport to the walls, where the atoms condense.

II. APPARATUS

The experimental setup is schematically shown in Fig. 2. We use a Janis model DT SuperVariTemp pumped helium cryostat. Optical access is provided via fused quartz windows, the innermost windows having the diameter of 1 in. A 2.5-in. tall cylindrical copper cell, with inner diameter of 1.25 in., is mounted inside the cryostat, in line with the windows. The cell prevents the ablated species from being deposited on the inside walls and windows of the cryostat sample space, which are hard to clean. The copper cell has four 1-in. diameter fused quartz windows, and several holes at the top and bottom to make sure that the buffer-gas pressure inside the cell is equal to that inside the cryostat sample space. The ablation target is mounted on a holder inside the cell. At the top of the cryostat, the sample space is connected to a Stokes Pennwalt rotary vane pump via a 3/4-in. diameter pumping arm. Also at the top, there is a connection to an MKS Baratron Type 220B pressure gauge and a valve for letting in buffer gas from a pressurized cylinder (99.995% purity). The temperature is monitored with a LakeShore silicon-diode temperature sensor, model DT-470-CU-13-1.4L, mounted on the top of the copper cell. The LakeShore model 321 controller, combined with a wound heater mounted next to the temperature sensor, allows temperature control during the experiment.

A Q-switched Spectra-Physics DCR-11 Nd:YAG laser, operating at the fundamental wavelength (1064 nm), is used to ablate the targets. The laser beam passes through a set of lenses to expand it (this is done to avoid damaging the cryostat windows by the focused beam), and is then focused to a spot on the ablation target by a large-numerical-aperture lens. The focus (the ablation spot) can be moved around the surface of the target by moving this lens, which is mounted on a three-coordinate translation stage. Several different ablation-laser operating regimes have been explored. It was found that the ablation yield is independent of pulse energy when it is above 30 mJ, but drops when the pulse energy is lower. Doubling the frequency of the ablation pulse and operating at 532 nm had no noticeable effect on the ablation yield. Firing the laser with the Q-switch disabled gave a "long" 100-μs light pulse. When such a pulse was used for ablation, the resulting atomic yield was at least an order of magnitude lower than that obtained with the Q-switched laser. After exploring these ablation regimes, the following parameters were chosen for data taking: pulse energy of 50 mJ, fundamental wavelength (1064 nm), Q-switched (10-ns light pulse).

III. SILVER AND GOLD

Four atomic species have been studied in our experiment: lithium, rubidium, silver, and gold. We start with the discussion of ablation of silver and gold. These atoms were chosen, on the one hand, because of their ground-state electronic configurations, consisting of a single s electron outside a filled shell. They have $S_{1/2}$ ground states, and their spectra are similar to those of alkali-metal atoms. On the other hand, unlike the alkali metals, silver and gold are ductile, and thin wires (diameter as small as 25 μm) are readily available. We decided to use such thin wires as ablation targets for the following reasons. The amount of material that has to be vaporized to create an atomic density of 10^{11} cm^{-3} inside the cell of volume 20 cm^3 is only 2×10^{12} atoms. The energy required to evaporate that amount of material is approximately 1 μJ. The rest of the energy delivered to the target by the ablation pulse goes into the buffer-gas shock wave, ejects macroscopic pieces of the target, or is conducted away into the bulk of the target, heating it up, and heating the buffer gas with it. Using the tip of a submillimeter diameter wire as the ablation target allows the heat conduction away from the ablation spot to be minimized, because the wire's cross-sectional area through which the heat escapes is small. In addition, the thin wire has a much smaller surface area than a flat target, so the probability of ablated atoms to diffuse back and stick to the target surface is minimized.

Silver and gold wires of 50 μm diameter (purchased from Alfa Aesar) were used as ablation targets. Measurements were also taken using wires of 25 and 100 μm diameter; wire thickness did not significantly affect experimental results in this range. The wire was mounted vertically in the middle of the cell inside the cryostat sample space, so that the tip of the wire was just below the center of the cell windows. Aiming the ablation laser focus at the tip of the wire was done as follows. The laser intensity was reduced by a neutral density filter to avoid ablation. When the wire was in the focus, it blocked part of the beam, and a shadow was clearly visible on the beam stop, where the laser beam was projected after it exited the cryostat. Once the laser was aimed directly at the wire tip, the neutral density filter was removed and an ablation shot was fired. As the material at the wire tip was evaporated, the ablation spot was moved up by translating the focusing lens.

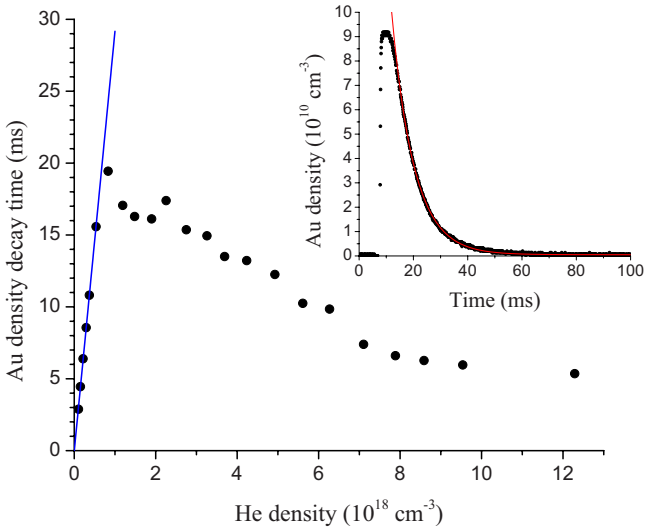

FIG. 3. (Color online) Gold-atom density decay time as a function of helium density at 295 K. The straight line is a linear fit to the low-helium-density data, where diffusion dominates the gold-atom loss. The scatter of the points is due to shot-to-shot fluctuations in the vapor production process. The inset shows the evolution of gold-atom vapor density after a single ablation shot, for helium density of 7×10^{18} cm^{-3}. The red line is an exponential fit to the density decay; the fitting range is from 15 to 100 ms.

Ablated atoms were detected by measuring the absorption of a light beam resonant with the $D1$ atomic transition. This light beam was produced by a hollow cathode lamp (HCL) and focused with a lens to a beam approximately 3 mm in diameter, defined by the pair of irises, one on either side of the cryostat. A narrow-band interference filter was used to select the $D1$ atomic line. For the silver HCL a 338-nm filter was used, and for the gold HCL a 270-nm filter was used. In each case the transmitted spectrum was measured with a Czerny-Turner grating spectrometer, confirming that only a single spectral line was present. We also checked that the observed signal was indeed resonant atomic absorption rather than some broadband scattering: when a helium-neon laser beam was used as the probe in place of the HCL, no absorption was detected.

The inset in Fig. 3 shows the time evolution of gold-atom density after a single ablation shot is fired into the tip of the gold wire. Gold atoms fill the cell after the ablation laser pulse. The photodetector bandwidth is not wide enough to make an accurate measurement of the filling time. This time is faster than 100 μs and, in the entire experimental range of buffer-gas densities, is always much faster than the time it would take for Au atoms to diffuse from the wire to the location of the probe beam, which is 5 mm away. The filling process must be nondiffusive—a shock wave propagates in the helium gas after the ablation pulse, filling the cell with

ablated Au atoms. Typical Au densities achieved are on the order of 10^{11} cm^{-3}. After a maximum is reached, the atomic density starts to decrease. Exponential decay fits the data well, and the loss of Au atoms from the buffer gas can be characterized by the corresponding decay time. The mechanisms causing this Au atom density decay are discussed below.

The evolution of Au atom density after an ablation shot at each helium density and room temperature were recorded, and the resulting decay times are plotted in Fig. 3. At small helium density, the Au loss time grows linearly with helium density. In this regime, Au loss due to diffusion to the cell walls dominates. The atoms are lost at the walls since the temperature is too low to support any significant Au vapor pressure. An estimate for the diffusion time t_d can be approximated as the decay time of a fundamental diffusion mode in a cylindrical cell of radius R:

$$t_d \simeq \frac{R^2}{6D}, \tag{6}$$

where D is the diffusion coefficient $D \simeq \lambda v/3 \simeq v/3\sigma_t n_{\mathrm{He}}$. Here λ is the mean free path of Au atoms, σ_t is their transport cross section, v is the r.m.s. relative velocity, and n_{He} is the helium density. The diffusion time can be expressed as

$$t_d \simeq \frac{R^2\sigma_t}{2v} n_{\mathrm{He}}. \tag{7}$$

Indeed the diffusion time grows linearly with increasing helium density, and the diffusion coefficient D_{AuHe} for gold atoms in helium can be extracted from the slope. The result for the temperature of 295 K and atmospheric pressure is $D_{\mathrm{AuHe}} \simeq 0.5$ cm^2/s (which corresponds to a reasonable value of the transport cross section $\sigma_t \approx 10^{-15}$ cm^2). No published value for this diffusion coefficient has been found in literature.

If diffusion to the walls were the only loss mechanism, Au vapor lifetime would continue to grow linearly with increasing helium density, and reach about a second at the density of $\approx 3 \times 10^{19}$ cm^{-3}. As evident from Fig. 3, however, at helium density of about 10^{18} cm^{-3} another Au loss mechanism starts to dominate, and the Au vapor lifetime decreases with increasing helium pressure. One candidate for this loss is dimer formation $\mathrm{Au}+\mathrm{Au} \rightarrow \mathrm{Au}_2$. When such a dimer is formed, the Au atoms are lost, since they are no longer resonant with the probe laser. A collision between two gold atoms in vacuum cannot form a dimer, since both energy and momentum cannot be conserved in such a process. A third body is needed, and a helium atom can fulfill this role if it is close enough to the colliding Au atoms. Dimer formation rate then grows with growing helium density, and this can explain the decrease of gold lifetime as helium density increases. However, simple estimates predict dimer formation rates that are about an order of magnitude too small to explain the observed gold-atom loss. In addition, if dimer formation dominated the atom loss, the time dependence of the density decay would be nonexponential; instead $n(t)=a/(t-t_0)$ would be

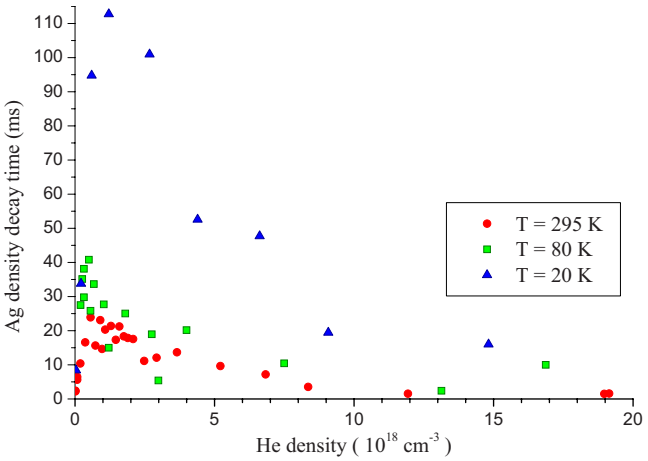

FIG. 4. (Color online) Silver vapor density decay time as a function of helium buffer-gas density at different temperatures.

the correct solution (with fitting constants a and t_0), and the available experimental data do not show evidence of such time dependence.

Another possible gold-atom loss mechanism is capture by clusters $\mathrm{Au}+\mathrm{Au}_k \rightarrow \mathrm{Au}_{k+1}$. For this process there is no need to have a helium atom nearby, since excess kinetic energy can be converted into vibrational energy of the cluster and subsequently carried away by collisions of the cluster with helium atoms. Hence there is no dependence of the cross section on the helium density. The interaction between a gold atom and a cluster is well described by the van der Waals potential, and, as a consequence of high cluster polarizabilities, the cross sections are extremely large, on the order of 10^{-13} cm^2, for clusters with $k \simeq 10$ [26]. If we take this value as the gold-atom capture cross section, the number density of clusters required to produce gold-atom loss on the time scale of 10 ms is 10^{11} cm^{-3}. Where would these clusters come from? As argued previously, dimer formation is too slow to lead to nucleation of an appreciable number of clusters. The ablation process itself, however, is likely to produce such clusters [27,28]. As the ablation laser hits the target, it locally heats the material, creating an explosion. The explosion forms a shock wave, which expands out into the helium gas. Some of the high-density gold vapor created by the explosion condenses into clusters in the low-pressure region behind the shock. The higher the helium density, the greater the efficiency of this condensation, the more clusters are produced, and the faster the rate of gold vapor loss. This may explain the trend observed in Fig. 3.

The third possible loss mechanism is capture of a gold atom by an impurity (such as a hydrocarbon or an oxide molecule) that is either present in the buffer gas to start with, or gets ablated off the target surface. Such an impurity can easily have a large capture cross section, and the impurity density of 10^{11} cm^{-3} or more is not at all implausible.

A study of the temperature dependence of the atomic vapor lifetime was performed using silver atoms. The silver vapor-density decay times are plotted in Fig. 4 for laser ablation of a 50-μm-diameter silver wire in helium buffer gas at three temperatures. The trends are similar to the ones in Fig. 3, where gold vapor results are shown. At small helium

density, the silver vapor lifetime grows linearly, and the main atom loss mechanism is diffusion to the cell walls. The diffusion coefficient D_{AgHe} for silver atoms in helium can be extracted from the slope of the linear dependence of diffusion time on helium density, using Eq. (6). The result for the temperature of 295 K and atmospheric pressure is $D_{\mathrm{AgHe}} \simeq 0.4$ cm^2/s. Silver vapor lifetime reaches a maximum at $n_{\mathrm{He}} \simeq 10^{18}$ cm^{-3} and decreases for larger helium densities. The silver-atom loss mechanisms are likely the same as those for gold, described above. It can be seen in Fig. 4 that at low temperatures, longer atomic vapor lifetimes can be achieved. This is mostly due to lower atomic thermal velocities $v \propto \sqrt{T}$, leading to smaller diffusion constants at lower temperature. The longest observed silver vapor lifetime was 113 ms at the temperature of 20 K [29]. The peak silver atomic densities were on the order of 10^{11} cm^{-3}. Data were also taken at 80 and 295 K with three other buffer gases: nitrogen, neon, and argon. It was found that the atomic-vapor decay time at a given buffer-gas density does not noticeably depend on which of these buffer gases is used.

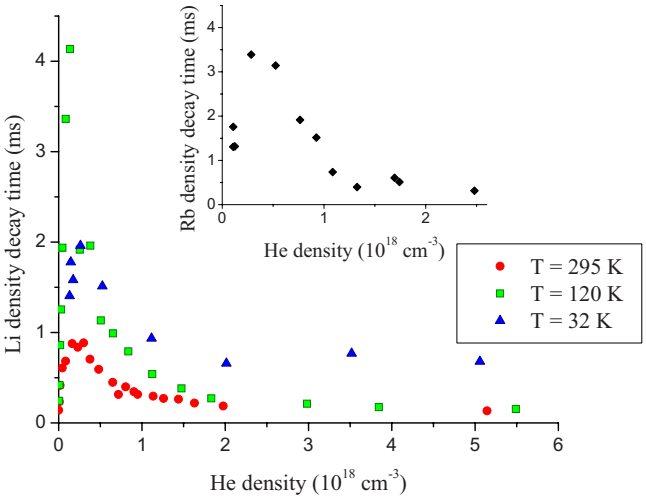

FIG. 5. (Color online) Lithium vapor density decay time as a function of helium buffer-gas density at different temperatures. The inset shows rubidium data at 295 K.

IV. LITHIUM AND RUBIDIUM

Studying silver and gold atoms is difficult because their atomic transition frequencies lie in the ultraviolet: the $D1$ lines are at the wavelengths of 338 nm for silver and 268 nm for gold. The hollow-cathode lamps are sufficient for absorption measurements, but for optical pumping a more intense light source is needed. Such light sources (diode lasers) are readily available for alkali-metal atoms. We therefore undertook a study of alkali-metal-atom ablation with our experimental setup. Experiments with lithium and rubidium were performed. For lithium the ablation target was in the form of 0.75-mm thick and 19-mm wide lithium foil (purchased from Alfa Aesar), and for rubidium the target was a roughly 5-mm thick and 10-mm wide piece of pure rubidium metal. Alkali metals are extremely reactive, and they oxidize quickly when exposed to air. Therefore, ablation targets were prepared in a glove box with argon atmosphere. The target was mounted inside the copper cell, level with the cell windows. The glove box was then opened and the cell was quickly inserted into the cryostat, which was immediately pumped out. In this way the exposure of the alkali-metal targets to air was minimized.

Ablated atoms were detected by measuring the absorption of a laser beam resonant with one of the $D1$ or $D2$ atomic transitions. Lithium atoms were probed with the light from a 671-nm laser diode (TOLD 9221M) inside a temperature-controlled mount (Thorlabs TCLDM9) paired with a TED-200 temperature controller and a LDC-201-ULN current controller. The laser beam diameter was approximately 2 mm. A 750-MHz free spectral range confocal Fabry-Perot (FP) spectrum analyzer was used for spectral diagnostics of the laser light. Tuning to the ^{7}Li (92.5% abundance) $D1$ resonance line at 671 nm was achieved by splitting off a part of the beam, modulating the intensity with a chopper wheel at 350 Hz, and aiming it into the cathode of a lithium hollow-cathode lamp (HCL). When the laser was tuned to the lithium resonance, the HCL current was modulated at the chopper frequency (optogalvanic effect) [30]. This modulation was detected with a lock-in amplifier, referenced to the chopper-wheel frequency. The setup for rubidium atoms was similar, with the 671-nm laser diode replaced with a 780-nm laser diode, and the hollow cathode lamp replaced with a rubidium vapor cell, which was used to tune the laser to the Rb $D2$ transition by detecting atomic fluorescence.

The time evolution of lithium and rubidium atom density after an ablation shot is very similar to that shown on the inset in Fig. 3 for gold. The ablated atoms fill the cell very quickly after the laser pulse, a maximum is reached, and then the atomic density decreases. Exponential decay fits the data well, and the decay times are plotted in Fig. 5 for lithium in a range of temperatures. Rubidium data at room temperature are shown in the inset. The trends are the same as those seen for gold and silver atoms. At low helium density the vapor loss time increases linearly, in agreement with Eq. (7), which describes diffusion to the walls. However, the maximum in the decay time now occurs at lower helium density, of approximately 0.2×10^{18} cm^{-3}. At higher densities another loss mechanism dominates, keeping the decay times short. As discussed above, the possible candidates for this mechanism are dimer formation, atom loss on sputtered clusters, and atom loss on impurities in the buffer gas. For an unknown reason, this mechanism is more efficient for alkali-metal atoms than for silver and gold [31]. This leads to shorter vapor loss times for the alkali metals, on the order of 4 ms at the maximum. Curiously, the longest lithium vapor lifetime was obtained at the temperature of 120 K, rather than 32 K. Data were also taken at 295 K with nitrogen as the buffer gas. It was found that the lithium vapor decay time at a given buffer gas density does not noticeably depend on whether the buffer gas is helium or nitrogen.

V. CONCLUSIONS AND OUTLOOK

In conclusion, we have used laser ablation to create and study atomic vapors of silver, gold, lithium, and rubidium inside helium and other buffer gases in a wide range of tem-

peratures and buffer-gas pressures. Vapor densities of 10^{11} cm^{-3} have been achieved. The longest measured atomic vapor lifetimes are on the order of 110 ms for silver [29] and 4 ms for lithium. For buffer-gas density $n \ll 10^{18}$ cm^{-3} the atomic vapor loss is dominated by diffusion to the cell walls, where the atoms condense. Increasing the buffer-gas density above 10^{18} cm^{-3}, however, does not increase the atomic vapor lifetime; instead the lifetime gets shorter. The possible loss mechanisms that can cause this behavior are dimer formation, atom loss on clusters created during the ablation process, or atom loss on impurities in the buffer gas.

To put our results in context, let us consider the figure of merit of an atomic magnetometer, or any shot-noise limited precision measurement with an ensemble of N atoms with coherence time τ [2,32]:

$$\mathrm{FOM} \propto \sqrt{N\tau}. \tag{8}$$

The coherence times have not been measured in our experiments so far (these measurements are currently in progress). However, as argued at the beginning of this paper, the buffer-gas collisional relaxation rates at cryogenic temperatures are expected to be on the order of mHz. If atom loss as measured in our experiments proves to be the dominant mechanism for coherence relaxation, then coherence relaxation rates on the order of several hertz are expected. With atomic vapor densities of 10^{11} cm^{-3} already demonstrated, the figure of merit for our system is competitive with the leading atomic magnetometers today [2]. Our setup, however, has the advantage of operation in a wide range of temperatures: from 4 to 300 K, while the vapor-cell based measurements can only be performed at room temperature and above.

ACKNOWLEDGMENTS

The authors thank Valeriy Yashchuk and Max Zolotorev for many useful discussions. This research was supported by the National Science Foundation through Grant No. 055 4813.

[1] D. Budker, W. Gawlik, D. F. Kimball, S. M. Rochester, V. V. Yashchuk, and A. Weis, Rev. Mod. Phys. **74**, 1153 (2002).
[2] D. Budker and M. Romalis, Nat. Phys. **3**, 227 (2007).
[3] W. Happer, Rev. Mod. Phys. **44**, 169 (1972).
[4] D. Bouwmeester, A. K. Ekert, and A. Zeilinger, *The Physics of Quantum Information: Quantum Cryptography, Quantum Teleportation, Quantum Computation*, 1st ed. (Springer, Berlin, 2000).
[5] C. J. Berglund, L. R. Hunter, D. Krause, E. O. Prigge, M. S. Ronfeldt, and S. K. Lamoreaux, Phys. Rev. Lett. **75**, 1879 (1995).
[6] T. W. Kornack and M. V. Romalis, Phys. Rev. Lett. **89**, 253002 (2002).
[7] I. B. Khriplovich and S. K. Lamoreaux, *CP Violation without Strangeness* (Springer-Verlag, Berlin, 1997).
[8] M. A. Bouchiat and J. Brossel, Phys. Rev. **147**, 41 (1966).
[9] E. B. Alexandrov, M. V. Balabas, A. S. Pasgalev, A. K. Vershovskii, and N. N. Yakobson, Laser Phys. **6**, 244 (1996).
[10] D. Budker, V. Yashchuk, and M. Zolotorev, Phys. Rev. Lett. **81**, 5788 (1998).
[11] R. A. Bernheim, J. Chem. Phys. **36**, 135 (1962).
[12] S. Brandt, A. Nagel, R. Wynands, and D. Meschede, Phys. Rev. A **56**, R1063 (1997).
[13] M. Erhard and H. Helm, Phys. Rev. A **63**, 043813 (2001).
[14] Z. Wu, T. G. Walker, and W. Happer, Phys. Rev. Lett. **54**, 1921 (1985).
[15] T. G. Walker, J. H. Thywissen, and W. Happer, Phys. Rev. A **56**, 2090 (1997).
[16] E. I. Dashevskaya and E. A. Kobzeva, Opt. Spektrosk. **30**, 807 (1971).
[17] T. G. Walker, Phys. Rev. A **40**, 4959 (1989).
[18] C. Zhu, A. Dalgarno, S. G. Porsev, and A. Derevianko, Phys. Rev. A **70**, 032722 (2004).
[19] G. Herzberg, *Molecular Spectra and Molecular Structure. I. Spectra of Diatomic Molecules* (van Nostrand, New York, 1950).
[20] W. C. Chen, T. R. Gentile, T. G. Walker, and E. Babcock, Phys. Rev. A **75**, 013416 (2007).
[21] A. Hatakeyama, K. Oe, K. Ota, S. Hara, J. Arai, T. Yabuzaki, and A. R. Young, Phys. Rev. Lett. **84**, 1407 (2000).
[22] A. Hatakeyama, K. Enomoto, N. Sugimoto, and T. Yabuzaki, Phys. Rev. A **65**, 022904 (2002).
[23] S. E. Maxwell, N. Brahms, R. deCarvalho, D. R. Glenn, J. S. Helton, S. V. Nguyen, D. Patterson, J. Petricka, D. DeMille, and J. M. Doyle, Phys. Rev. Lett. **95**, 173201 (2005).
[24] J. Kim, B. Friedrich, D. P. Katz, D. Patterson, J. D. Weinstein, R. DeCarvalho, and J. M. Doyle, Phys. Rev. Lett. **78**, 3665 (1997).
[25] R. deCarvalho, J. M. Doyle, B. Friedrich, T. Guillet, J. Kim, D. Patterson, and J. D. Weinstein, Eur. Phys. J. D **7**, 289 (1999).
[26] V. V. Kresin, G. Tikhonov, V. Kasperovich, K. Wong, and P. Brockhaus, J. Chem. Phys. **108**, 6660 (1998).
[27] W. T. Nichols, G. Malyavanatham, D. E. Henneke, D. T. O'Brien, M. F. Becker, and J. W. Keto, J. Nanopart. Res. **4**, 423 (2002).
[28] S. I. Anisimov and B. S. Luk'yanchuk, Phys. Usp. **45**, 293 (2002).
[29] Recently, measurements at slightly different experimental conditions (lower temperatures, for example) showed even longer silver-atom lifetimes, up to 300 ms.
[30] D. S. King and P. K. Schenck, Laser Focus (Newton, Mass.) **14**, 50 (1978).
[31] This may be due to the fact that only bulk targets were used for alkali-metal ablation, while sub-mm diameter wires were the targets for silver and gold. On the other hand, as mentioned in Sec. III, the wire diameter (in the range 25 to 100 μm) did not noticeably affect experimental results for silver and gold.
[32] M. Auzinsh, D. Budker, D. F. Kimball, S. M. Rochester, J. E. Stalnaker, A. O. Sushkov, and V. V. Yashchuk, Phys. Rev. Lett. **93**, 173002 (2004).